Article:
Liu, C, Yue, M, Banwart, SA et al. (2022) Kinetic Modeling for a Novel Permeable Reactive Biobarrier for In Situ Remediation of PAH-Contaminated Groundwater. Journal of Geotechnical and Geoenvironmental Engineering, 148 (5). ISSN: 0733-9410

https://doi.org/10.1061/(ASCE)GT.1943-5606.0002779

Kinetic modelling for a novel permeable reactive bio-barrier for in-situ remediation of PAH-contaminated groundwater

Cuicui Liu[a,b], Yue Ma[c], Steven A. Banwart[d,e], Xiaohui Chen[f]*, Wenchao Du[g], Ying Yin[h], Hongyan Guo[i,]*

[a]State Key Laboratory of Pollution Control and Resource Reuse, School of the Environment, Nanjing University, Nanjing, 210023, China

[b]School of Civil Engineering, University of Leeds, Leeds, LS2 9JT, UK

[c]School of Civil Engineering, University of Leeds, Leeds, LS2 9JT, UK

[d]School of Earth and Environment, University of Leeds, Leeds, LS2 9JT, UK

[e]Global Food and Environment Institute, University of Leeds, Leeds, LS2 9JT, UK

[f]School of Civil Engineering, University of Leeds, Leeds, LS2 9JT, UK

[g]School of the Environment, Nanjing Normal University, Nanjing, 210023, China

[h]State Key Laboratory of Pollution Control and Resource Reuse, School of the Environment, Nanjing University, Nanjing, 210023, China

[i]State Key Laboratory of Pollution Control and Resource Reuse, School of the Environment, Nanjing University, Nanjing, 210023, China

*Correspondence: Xiaohui Chen and Hongyan Guo, tel.: +44(0)113 343 0350

E-mail: x.chen@leeds.ac.uk and hyguo@nju.edu.cn

Abstract

Permeable reactive barriers (PRBs) are an environmentally-friendly and cost-effective *in situ* remediation technology and have been used to restore polycyclic aromatic hydrocarbons (PAHs)-contaminated groundwater. However, the understanding of removal mechanisms of the pollutant from groundwater remains as a challenge due to the complex interactions between microbial evolution, organic carbon kinetics and multiple chemical reactions. In this study, a one-dimensional reactive transport model was developed to study 450-day column experiments for removal of phenanthrene from groundwater using new PRB materials A (including wheat straw) and B (including coconut shell biochar). The modelling results provided a deeper understanding of the removal process for phenanthrene that material B had a higher removal efficiency than A over 34 days. The removal efficiency of phenanthrene in both A and B was close to 100% in the PRB system. This is because: (1) Material B had a higher adsorption capacity for phenanthrene than material A. Adsorption played an important role in the short term (e.g. 20 days), whereas, biodegradation controlled longer-term removal processes. (2) The biomass in column B was higher ($p < 0.05$) than in column A. (3) B had a higher microbial yield coefficient that could favor longer-term microbial growth and biodegradation activity. Material B might have a greater potential than A for longer-term remediation performance. The simulated results were generally in agreement with the experimental results and supported the development of field-scale pilot testing of these materials for groundwater

remediation.

Keywords: Phenanthrene; PHREEQC; Kinetics; Permeable reactive barrier; Groundwater remediation

1. Introduction

Polycyclic aromatic hydrocarbons (PAHs) are potentially mutagenic and carcinogenic to humans (Ferreira et al. 2013). The groundwater in Northern, Northeastern, Southeastern, and Southwestern China is severely polluted by PAHs. Research has reported that PAHs can be biodegraded to CO_2 and H_2O by microbes under aerobic conditions and the biodegradation rate of PAHs can be influenced by dissolved oxygen (DO) levels (Haritash and Kaushik 2009; Waigi et al. 2015). The concentration of DO in groundwater is generally very low (< 3 mg/L) (Yeh et al. 2010). Hence, the biodegradation of PAHs may be limited by the low concentration of DO and by the relatively low solubility of PAHs in the aqueous phase. Therefore, the main challenges for *in situ* bioremediation of PAHs contaminated groundwater are the choice of a suitable carbon substrate and the supply of reactive oxygen species. Calcium peroxide (CaO_2) is an efficient oxygen-releasing compound, which could provide DO for the bioremediation of PAH-contaminated groundwater (Lin et al. 2017). Biochar is an economical and readily available carbonaceous porous material (Mohanty et al. 2018). Straw has already been utilized as a low-cost carbon source material for groundwater remediation (Zhang et al. 2017). Therefore, calcium peroxide and straw/biochar have potential to be used in combination for permeable reactive barriers (PRBs), but they have infrequently been used in PAHs biodegradation applications so far.

PRBs have been a mature remediation technology for the treatment of polluted

groundwater for decades (Basu and Johnson 2012). The removal efficiency of the pollutant using PRBs depends on the type of reactive media used and the removal mechanism. Studies have shown that PRBs can successfully remove various pollutants transported by groundwater flow, including heavy metals, chlorinated solvents, aromatic hydrocarbons, and pesticides (Gandhi et al. 2002). However, PRBs have not been widely used to remove PAHs due to the limited available reactive media (Cobas et al. 2014). Phenanthrene is the smallest characteristic unit of carcinogenic PAHs (Wang et al. 2020) and is one of the most abundant PAHs in aquatic ecosystems. The ubiquitous distribution of phenanthrene in the aquatic environment and its tendency for accumulation within organisms results in the potential for deleterious effects (Hannam et al. 2010). In our previous research, we developed novel PRB materials that relied on a microbial self-domestication mechanism to remediate phenanthrene-contaminated groundwater (Liu et al. 2019). Column experiments were conducted to investigate the suitability of novel PRB materials for remediation of PAH-contaminated groundwater, including the adsorption and biodegradation of phenanthrene, the duration of carbon and reactive oxygen release, and the change in the relative abundance of active microbial biomass.

The aim of the current work is to simulate the results of column experiments with the geochemical modelling code PHREEQC as a quantitative analysis framework to gain a deeper understanding of the removal process of phenanthrene from groundwater using PRB technology. The combined mechanism of adsorption and

89 biodegradation were responsible for phenanthrene removal in columns A and B. We
90 assumed that materials A and B firstly adsorbed phenanthrene from groundwater.
91 Then, phenanthrene was degraded by microorganisms with the increase of biomass in
92 columns A and B. The previous research has showed the potential of microorganisms
93 aerobically degrading phenanthrene, with DO as the terminal electron acceptor
94 (Moscoso et al. 2012). The calcium peroxide component of materials A and B could
95 efficiently provide oxygen for aerobic biodegradation of phenanthrene and the
96 oxidation of dissolved total organic carbon (TOC). The organic carbon was released
97 from straw or biochar, which may maintain the capacity of microbes to degrade
98 phenanthrene when the concentrations of phenanthrene were low. The dissolved
99 organic carbon in columns A and B was assumed to be the carbon and energy source
100 to support microbial growth.
101
102 **2. Material and methods**
103 **2.1. Experimental study**
104 A new PRB material was developed for the remediation of phenanthrene
105 contaminated groundwater. The PRB materials A and B were both pellets that had a
106 three-layer structure including a wood brick core, a packed layer, and an outer shell.
107 Materials A and B had the same reactive oxygen source (calcium peroxide), but with
108 different carbon source (wheat straw and coconut shell biochar). The diatomite,
109 attapulgite, and Portland cement in the materials served as adhesive components. The

materials were bound by sodium alginate mixed with water. Detailed information about the composition of the PRB material is given in Table 1.

A 450-day column experiment was conducted to assess the capacity of the new PRB materials to remove phenanthrene from groundwater. The length of glass columns was 50 cm and the inner diameter was 4 cm. Columns A and B were equipped with four sampling ports (named SP1-4) spaced at 10 cm intervals. The columns were packed with a homogenous mixture of either material A or B and quartz sand (1:1, v/v). The materials A and B in the columns were bounded by a 5 cm-layer sand at both the bottom and the top. The relatively high concentrations of phenanthrene in groundwater ranged from 0.2 to 1 mg/L (Broholm et al. 1999; Ebihara and Bishop 2002; Zhang et al. 2019). The flow rate was chosen to simulate typical flow conditions of shallow aquifers, which corresponded to a flow velocity of less than 2 m day^{-1} (Folch et al. 2013). The phenanthrene (0.9 mg/L) contaminated groundwater was pumped into the columns at a flow rate of 126.89 μL min^{-1} by the peristaltic pump. The corresponding flow velocity transported in the columns was about 0.48 m day^{-1}, which was less than 2 m day^{-1} noted for shallow groundwater flow. A total of 53.02 L per year of groundwater flowed through the column. The details of the columns are shown in Table 2.

The effluent of the columns was frequently sampled. The pH and DO were measured immediately after collecting the samples from the columns using a portable analyzer (Orion 5 Star, Thermo, USA). The TOC concentrations were determined

using a total organic carbon analysis meter (TOC-Aurora 1030D, OI, US). The phenanthrene concentrations were determined using high performance liquid chromatography (HPLC 1200, Agilent, USA). The details for phenanthrene adsorption experiments of materials A and B were shown in Liu et al. (2019). After the column experiments had run for 200 days, samples of the materials were collected from the sampling ports in columns A and B. Subsamples (0.5 g) were taken from these samples and the DNA was extracted using a FastDNA^{TM} SPIN Kit for soils. The V4 region of the bacterial 16S rRNA gene was amplified using the 515F (5'-GTGCCAGCMGCCGCGGTAA-3') and 806R (5'-GGACTACHVGGGTWTCTAAT-3') primers for pyrosequencing on a sequencer (MiSeq) (Caporaso et al. 2012; Caporaso et al. 2011).

2.2. Column experiments analysis and kinetic results

The modelling study considered the 450-day column experimental process, and focused on adsorption and microbial degradation processes for the removal of phenanthrene from groundwater. The kinetic information for the remediation of phenanthrene contaminated groundwater using the PRB system obtained from the literature is summarized below.

2.2.1. pH and dissolved oxygen

The materials A and B were assumed to gradually release calcium peroxide into the

flowing groundwater, which could cause the rise of pH value and the increase of dissolved molecular oxygen in the columns. The initial mass of CaO_2 in materials A and B were calculated as 0.330 and 0.315 mol, respectively. The reaction between CaO_2 and water can be described as follows:

$$2CaO_2 + 2H_2O \rightarrow 2Ca(OH)_2 + O_2 \quad (1)$$

The reaction equation of CaO_2 used in this paper is widely accepted in the literature and has been adopted by different authors investigating CaO_2 reaction both in experimental and modelling studies (Chen et al. 2012). The release rates of CaO_2 in A and B columns were assumed constant with value of 7.17×10^{-8} and 6.88×10^{-8} mol L^{-1} s^{-1}, respectively, so as to obtain the best fit of the model to the experimental data. The production rate of DO ($R_{ox} = \lambda$) in A and B columns based on equation (1) should be 3.58×10^{-8} and 3.44×10^{-8} mol L^{-1} s^{-1}, respectively.

2.2.2. Phenanthrene adsorption in columns A and B

The retardation of contaminants due to the process of adsorption can be modeled with a linear reversible sorption expression characterized by a constant distribution coefficient (defined below). The rate of phenanthrene adsorption is given by Tebes-Stevens et al. (1998):

$$R_{phen,sorp} = -k_m \left(C_{phen,pw} - \frac{C_{phen,s}}{K_d} \right) \quad (2)$$

where $R_{phen,sorp}$ is the adsorption rate (mol L^{-1} s^{-1}) of phenanthrene, $C_{phen,pw}$ denotes the aqueous concentration (mol L^{-1}) of phenanthrene, $C_{phen,s}$ denotes the

adsorbed concentration (mol g^{-1}) of phenanthrene, k_m is the mass transfer coefficient (s^{-1}), and K_d is the distribution coefficient (L g^{-1}) for the linear equilibrium adsorption. The value of k_m and K_d were obtained in accordance with the column-type modelling processes used to describe dynamic adsorption mass transfer (Pantić et al. 2019; Tebes-Stevens et al. 1998).

2.2.3. Phenanthrene biodegradation and biomass increase in columns A and B

The microbes could use organic carbon as a carbon and energy source, which is chemically defined in our modelling simulations as CH_2O. The degradation of organic carbon can be described by the reaction:

$$CH_2O + O_2 \rightarrow HCO_3^- + H^+ \quad (3)$$

The stoichiometric equation for the complete mineralization of phenanthrene is:

$$C_{14}H_{10} + 16.5O_2 \rightarrow 14CO_2 + 5H_2O \quad (4)$$

The gross growth of the biomass, μ (s^{-1}), is assumed to be limited by the availability of substrate and molecular oxygen, which is expressed with a multiple substrate Monod equation (Ai 2007; Berge et al. 2007; Geng et al. 2013; Wu et al. 2015):

$$\mu = \mu_{max,s} \frac{C_{s,pw}}{K_s + C_{s,pw}} \frac{C_{ox,pw}}{K_{ox} + C_{ox,pw}} \quad (5)$$

where $\mu_{max,s}$ is the maximum growth rate (s^{-1}), $C_{s,pw}$ is the aqueous concentration (mol L^{-1}) of the substrate (phenanthrene or TOC) as electron donor, K_s is the half-maximum rate concentration (mol L^{-1}) of the substrate, $C_{ox,pw}$ is dissolved molecular oxygen concentration (mol L^{-1}) as electron acceptor and K_{ox} is the

194 half-maximum rate concentration (mol L^{-1}) of DO. The dissolved molecular oxygen
195 was mainly consumed by the degradation of phenanthrene and the oxidation of
196 dissolved total organic carbon in columns A and B. The Monod kinetic parameters
197 (e.g. $\mu_{max,s}$, K_s, and K_{ox}) were taken from the studies related to the degradation of
198 organic compounds (Carboneras et al. 2017; Krishnan et al. 2017; Lokshina et al.
199 2001; McClure and Sleep 1996; Tebes-Stevens et al. 1998; Verce et al. 2000), which
200 could obtain the best fit of the model to the measured results.

201 The substrate consumption was assumed to be a function of the biomass
202 concentration (Carvajal et al. 2018; Geng et al. 2013; Safdari et al. 2018):

203 $$R_{s,bio} = \frac{dS}{dt} = -\frac{\mu}{Y_{X_S}} X_s \qquad (6)$$

204 where $R_{s,bio}$ is the rate (mol L^{-1} s^{-1}) of substrate consumption, μ is the gross growth
205 rate (s^{-1}) of the biomass, X_s is the concentration (mol biomass C L^{-1}) of biomass, Y_{X_s}
206 is microbial yield coefficient (mol biomass C/mol substrate C). The consumption rate
207 of phenanthrene and dissolved organic carbon can be defined as shown below,
208 respectively:

209 $$R_{phen,bio} = -\frac{\mu_{max,phen} X_{phen}}{14 Y_{X_{phen}}} \frac{C_{phen,pw}}{K_{phen}+C_{phen,pw}} \frac{C_{ox,pw}}{K_{ox}+C_{ox,pw}} \qquad (7)$$

210 $$R_{TOC,bio} = -\frac{\mu_{max,TOC} X_{TOC}}{Y_{X_{TOC}}} \frac{C_{TOC,pw}}{K_{TOC}+C_{TOC,pw}} \frac{C_{ox,pw}}{K_{ox}+C_{ox,pw}} \qquad (8)$$

211 The carbon content of the biomass was estimated using the carbon content per
212 bacterial cell (i.e. 9.4×10^{-14} g C/cell) (Acharya et al. 2019). The rate of biomass
213 accumulate or loss is dependent on the rate of substrate utilization and a first-order
214 decay rate for the biomass (Akobi et al. 2017). Therefore, the change rate of biomass

concentration on phenanthrene and dissolved organic carbon are given by the equations, respectively (Balakrishnan et al. 2019):

$$R_{bm,phen} = -14Y_{X_{phen}}R_{phen,bio} - bX_{phen} \quad (9)$$

$$R_{bm,TOC} = -Y_{X_{TOC}}R_{TOC,bio} - bX_{TOC} \quad (10)$$

where $R_{bm,phen}$ is the rate (mol biomass C L^{-1} s^{-1}) of biomass growth on phenanthrene, $R_{bm,TOC}$ is the rate (mol biomass C L^{-1} s^{-1}) of biomass growth on TOC, b is first-order microbial decay coefficient (s^{-1}).

The yield coefficient Y_{X_s} links microbial growth to carbon consumption. It is defined as the ratio of organic carbon incorporated into cell mass in a given time interval to the total organic carbon consumption. The values of $Y_{X_{phen}}$ for phenanthrene in columns A and B were selected as 0.44 and 0.53, respectively. The $Y_{X_{TOC}}$ for dissolved organic carbon in columns A and B were defined as 0.932 and 0.954, respectively. The values of Y_{X_s} were adjusted based on inspection of the fit of simulation results to experimental data. The first-order biodecay is appropriate only when the substrate is the growth-limiting factor and the bacterial concentration is relatively high. The value of microbial decay rate was obtained based on Chen and McTernan (1992), who suggested the b value for bacteria.

2.3. Modelling approach

The PHREEQC Interactive Program (version 3.4.0.12927) is available from the U.S. Geological Survey, which is based on an ion-association equilibrium aqueous

236 speciation model and has capabilities for batch-reaction and one-dimensional (1-D)
237 transport calculations (Boluda-Botella et al. 2014). With respect to the numerical
238 method for transport modelling, PHREEQC can simulate several one-dimensional
239 transport processes: diffusion, advection, and dispersion, as well as advection and
240 dispersion with diffusion into stagnant zones. The wateq4f database of PHREEQC
241 was used to calculate the chemical speciation of major elements in the study (Bartzas
242 and Komnitsas 2010).

243 The conceptual model was established according to information from both
244 theoretical and experimental analysis. Fig. 1 shows a schematic diagram of the
245 column experiment processes and the major physiochemical and biological
246 mechanisms involved. Adsorption and microbial degradation processes for
247 phenanthrene were considered in the model. It was assumed that the consumption of
248 dissolved organic carbon attributed to supporting the growth of microorganisms as
249 carbon source. The calcium peroxide as oxygen source supported the biodegradation
250 of phenanthrene and the oxidation of dissolved organic carbon. According to the
251 conceptual model, the transport processes considered in the model were simulated
252 using the advection-dispersion reaction (ADR) equation:

253 $$\frac{\partial C_i}{\partial t} = -v\frac{\partial C_i}{\partial x} + D_L\frac{\partial^2 C_i}{\partial x^2} + \sum_{m=1}^{n} R_{im} \qquad (11)$$

254 where: C is the concentration of species in water (mol L^{-1}), i represents the different
255 species, t is time (s), v is pore water flow velocity (m s^{-1}), x is distance (m), D_L
256 is the hydrodynamic dispersion coefficient (m^2 s^{-1}, $D_L = D_e + \alpha_L v$, with D_e the

257 diffusion coefficient, and α_L the dispersivity (m)), n is the total number of reactions,
258 and R_{im} is the reaction rate (mol L^{-1} s^{-1}) or (mol biomass C L^{-1} s^{-1}). The term $v\frac{\partial C_i}{\partial x}$
259 represents advective transport, $D_L\frac{\partial^2 C_i}{\partial x^2}$ gives dispersive transport. The ADR equations
260 for the local change of species concentrations in porewater or solids are presented in
261 Table 3. The Cauchy boundary condition (Type 3 or flux) (Eq. (12)) was specified for
262 both inlet and outlet boundaries.

263 $$C(x_{end},t) = C_0 + \frac{D_L}{v}\frac{\partial C(x_{end},t)}{\partial x} \quad (12)$$

264 where C is the concentration in water (mol L^{-1}), t is time (s), v is the pore-water
265 flow velocity (m s^{-1}), x is distance (m), D_L is the hydrodynamic dispersion
266 coefficient (m^2 s^{-1}). A flux was used as the groundwater flow boundary condition at
267 the start and end cells. There were no measured values for diffusion coefficients and
268 dispersivity in the experiment. A value of 0.5 cm was defined for dispersivity which
269 was in the common range of column scales (Kohfahl and Pekdeger 2006). The
270 diffusion coefficient was assumed to be 0.03×10^{-9} m^2 s^{-1} (Obiri-Nyarko et al. 2015).
271 The model transport parameters are showed in Table 4.

272 The transport of the pollutant solution in columns was divided computationally into
273 10 equal cells in series along the column, in which the solution advected with a fixed
274 residence time in each cell. The core blocks using in the PHREEQC code included
275 SOLUTION, PHASES, REACTION, RATES, KINETICS, and TRANSPORT. The
276 reaction and kinetics parameter values (Table 5) were obtained from either the
277 experiment or published literature, which were utilized to define the model. The

modelling results for the values of state variables pH, DO, TOC, and phenanthrene concentrations were collated from results for the final cell of the columns (cell 10), which was corresponding to the experimental results in the effluent of columns A and B. In the simulations, in order to further assess the removal capacity of the columns for phenanthrene. The phenanthrene concentration of the initial solution was set to 0.9, 1.5, 2, and 2.5 mg/L, respectively. The simulated results for the biomass were collated from results for the cells 1, 4, 7, and 9, which were compared with the experimental results of the biomass from SP1-SP4 of columns A and B. The results of the model calculations were compared with the experimentally measured results. The findings from the numerical modelling and theoretical analysis were combined to provide a deeper quantitative understanding of phenanthrene removal processes from groundwater using PRB technology with these materials.

3. Results and discussion

3.1. Modelling of column experiments

The processes of the conceptual model for the column experiments have been mathematically modelled using the mixed equilibrium reaction and kinetics approach with the PHREEQC code. Changes in pH value, DO, TOC, phenanthrene concentration, and biomass, as measured in the column experiment, have been analyzed as state variables in the modelling simulations.

3.1.1. pH value and DO

The modelling and experimental results for pH and DO in the effluent of columns A and B are displayed in Figs. 2a-b. The pH value and DO concentration of the initial solution was about 7.0 and 0.14 mmol/L, respectively. The experimental results showed that the pH in the effluent of columns A and B was between 9.82 and 10.94, likely because $Ca(OH)_2$ formed from the CaO_2, and caused the pH to rise. The high pH may cause the inhibition of the microbial growth and biological enzyme activity (Zhang et al. 2018). The addition of the phosphate buffer may be able to neutralize the high pH (Lee and Fan 2020). The DO concentration in the effluent of columns A and B ranged from 0.19 to 0.32 mmol/L, which was higher than the initial solution. These data indicated that the CaO_2 incorporated in materials A and B acted as a slow-release source of DO. Sponza and Gok (2011) reported that the DO concentrations for the treatment of phenanthrene contaminated wastewater were between 0.125 and 0.188 mmol/L. Thus, the dissolved oxygen was enough for aerobic degradation of phenanthrene in the columns. The modelling results exhibited DO concentrations in columns A and B that rapidly increased to 0.28 and 0.29 mmol/L due to the chemical reaction between calcium peroxide and water causing the production of DO, respectively, on the 30th day. After that, the DO concentrations of columns A and B remained at about 0.28 and 0.29 mmol/L, respectively, because of the continuous release of calcium peroxide from materials. The pH value of columns A and B changed from 7.0 to 10.76 in the modelling results. Consequently, the modelling

320 results of pH and DO for columns A and B were in agreement with the experimental
321 results.
322
323 **3.1.2. TOC**
324 Fig. 2c provides the information about the modelling and experimental data of TOC in
325 the effluent of columns A and B. For the experimental results, the TOC concentration
326 of column A increased significantly and reached 41.7 mmol/L in the beginning, but
327 then dropped and was between 11.5 and 15.3 mmol/L in the remainder of the
328 experiment. This was assumed to occur because the wheat straw decomposition was
329 determined by the soluble fraction of the chemical components of straw during the
330 early stages, and then, it was largely dependent on mineralization of the insoluble
331 pool of straw (Cogle et al. 1989). However, the TOC concentration of column B
332 remained relatively stable and ranged from 6 to 16.3 mmol/L. In the simulation, the
333 initial TOC concentration in columns A and B was defined as 15.8 and 16.4 mmol/L,
334 which was calculated according to the TOC concentration (12.94 mmol/L) of the
335 initial solution and the organic carbon released from the materials A (1.79 g C) and B
336 (2.17 g C) each year. The modelling results showed that the TOC concentrations of
337 columns A and B increased to 15.12 and 15.51 mmol/L on the 34th day, respectively.
338 Then, the TOC concentrations of columns A and B began to decrease due to the
339 consumption as a carbon and energy source supporting the microbial growth. Based
340 on these results, we concluded that the TOC concentrations from the modelling results

were primarily consistent with the experimental results. However, the trend in the release of organic carbon from columns A and B could not be accurately simulated. It was difficult to parameterise relevant rate equations for the release process of organic carbon from columns A and B, so we simulated the consumption of organic carbon to represent the change of organic carbon in columns A and B.

3.1.3. The change of phenanthrene concentration

The modelling and experimental results of phenanthrene concentration in the effluent of columns A and B are depicted in Fig. 2d. The concentration of phenanthrene in the effluent of columns A and B was not detected during the entire experiment. The modelling results showed that the removal efficiency of phenanthrene was higher in column B than in column A over 34 days. The phenanthrene concentration in columns A (0.30 μmol/L) and B (0.06 μmol/L) reached a peak value on day 20. Then, the phenanthrene concentrations in columns A and B both decreased to levels near 0.01 μmol/L, and showed no significant change in the remaining duration of the experiment. The simulated results showed that the change in phenanthrene concentrations in the columns was generally in good agreement with the experimental results. Figs. 3a-c shows the modelling results for the change in phenanthrene concentration in the effluent of columns A and B when the simulated initial concentration of phenanthrene is 0.9, 1.5, 2, and 2.5 mg/L, respectively. With the increase of phenanthrene concentration in the initial solution, the peak phenanthrene

362 concentration in the effluent of columns A and B was also larger (Figs. 3a-b). The
363 removal efficiency of phenanthrene was also higher in column B than in column A in
364 the initial stage (Fig. 3c). The peak of the change in phenanthrene concentration was
365 observed in modelling results but was not appeared in the experimental results. The
366 phenanthrene adsorption experiments showed that the maximum adsorption capacities
367 of materials A and B for phenanthrene were 0.013 and 0.035 mg/g, respectively (Liu
368 et al. 2019). Columns A and B contained 250.5 and 238.5 g of material, respectively.
369 Therefore, it could be calculated that the maximum amounts of phenanthrene
370 adsorbed by columns A and B were 3.26 and 8.35 mg, respectively. A total of 58.3 mg
371 of phenanthrene passed through the column over the 450 days of operation, which
372 suggested that there was significant degradation of phenanthrene within the column.
373 Therefore, the observation for the change of phenanthrene concentrations in the
374 modelling results may be explained by the removal of phenanthrene in columns A and
375 B being mainly dependent on adsorption at the beginning, thereby the value displayed
376 a gradually increasing trend with time to adsorption equilibrium. In the following
377 section, the results showed that the phenanthrene concentration in columns A and B
378 began to drop with the increase of biomass, and was kept at a very low value in the
379 remaining experimental period. This indicated that adsorption potentially played an
380 important role in a short term (e.g. 20 days), whereas, biodegradation controlled
381 longer-term removal processes.
382

3.1.4. Biomass growth

The simulated and experimental results for the change of biomass in SP1-SP4 of columns A and B are shown in Figs. 4a-d. The trend of biomass of columns A and B obtained from the experimental results increased from SP1 to SP2 and decreased from SP2 to SP4 along the flow path in the column. This phenomenon could be explained that the sufficient DO and carbon source supported the rapid growth of microbes from SP1 to SP2, but the gradually increased pH in the columns inhibited the microbial growth from SP2 to SP4. The modelling results for the biomass of SP1-SP4 of the columns had a similar trend as the experimental results, which also increased with distance from the influent end of the column and then subsequently dropped (Figs. 4a-b). Moreover, the modelling and experimental results both showed that the biomass in samples from ports SP1-SP3 of columns A ($p < 0.01$) and B ($p < 0.01$) were respectively higher than those in the initial materials A and B. In addition, the biomass in column B was higher ($p < 0.05$) than in column A (Figs. 4c-d), which meant that material B was more suitable for microbial growth than material A. These data suggested that the modelling results were generally in agreement with the experimental results. The microbial yield coefficient (Y_X) of column B was also higher than column A. Therefore, column B might have a greater potential for supporting microbial growth.

3.2. Limitations and challenges of modelling the column experiment

Whether the column experiment could be simulated sufficiently well by numerical methods depends on: (1) the experimental data obtained; (2) the modelling tools and methods; (3) the theoretical analysis; (4) the relationship between the experiment and modelling. One of the challenges of simulating the column experiment was that it was difficult to exactly model the slow-release of organic carbon from materials A and B due to the lack of related experimental data. In order to achieve a reasonably accurate agreement between experimental data and simulation results for TOC, we simulated the consumption of organic carbon to represent the change of organic carbon in columns A and B.

4. Conclusions

The removal process of phenanthrene from groundwater using PRB technology including adsorption and biodegradation was simulated with a reactive transport model based on the PHREEQC code and the simulation results were generally in agreement with the experimental results. The results of numerical simulations showed a deeper understanding of the removal process for phenanthrene in columns A and B, and predicted that B had a higher removal efficiency than A before 34 days. The removal efficiency of phenanthrene in both A and B was close to 100% in the PRB system. Based on the conceptual model and simulation results, adsorption played an important role in a short term, however, biodegradation controlled longer-term phenanthrene removal processes. Additionally, the content of the biomass in column

B was higher ($p < 0.05$) than in column A, which indicated that material B was more suitable for microbial growth than material A. Therefore, material B might have a greater potential for effective biodegradation than material A in the longer term.

Data Availability Statement

Some or all data, models, or code that support the findings of this study are available from the corresponding author upon reasonable request.

Acknowledgments

We gratefully acknowledge the National Key R&D Program of China (2018YFD0800201 and 2018YFC1800806), the Environmental Protection Department of Jiangsu Province of China (Grant No. 2017001-1), and the Jiangsu Provincial Water Resources Department (Grant No. 2019064) for their financial support. Cuicui Liu was supported by the China Scholarship Council (No. 201806190133).

References

Acharya, K., Werner, D., Dolfing, J., Meynet, P., Tabraiz, S., Baluja, M.Q., Petropoulos, E., Mrozik, W., Davenport, R.J. 2019. "The experimental determination of reliable biodegradation rates for mono-aromatics towards evaluating QSBR models." *Water Res.* 160: 278-287.

446 Ai, S.B. 2007. "Traveling waves in a bioremediation model." *SIAM J. Appl. Math*. 68
447 (3): 680-693.
448 Akobi, C., Hafez, H., Nakhla, G. 2017. "Impact of furfural on biological hydrogen
449 production kinetics from synthetic lignocellulosic hydrolysate using mesophilic and
450 thermophilic mixed cultures." *Int. J. Hydrog. Energy* 42 (17): 12159-12172.
451 Balakrishnan, A., kameswari Kanchinadham, S.B., Kalyanaraman, C. 2019.
452 "Evaluation and kinetic study on enzyme supplementation to biological treatment of
453 vegetable tanning process wastewater." *Int. J. Environ. Sci. Technol*. 16 (10):
454 5945-5954.
455 Bartzas, G., Komnitsas, K. 2010. "Solid phase studies and geochemical modelling of
456 low-cost permeable reactive barriers." *J. Hazard. Mater*. 183 (1-3): 301-308.
457 Basu, A., Johnson, T.M. 2012. "Determination of hexavalent chromium reduction
458 using Cr stable isotopes: isotopic fractionation factors for permeable reactive barrier
459 materials." *Environ. Sci. Technol*. 46 (10): 5353-5360.
460 Berge, N.D., Reinhart, D.R., Dietz, J.D., Townsend, T. 2007. "The impact of
461 temperature and gas-phase oxygen on kinetics of in situ ammonia removal in
462 bioreactor landfill leachate." *Water Res*. 41 (9): 1907-1914.
463 Boluda-Botella, N., Valdes-Abellan, J., Pedraza, R. 2014. "Applying reactive models
464 to column experiments to assess the hydrogeochemistry of seawater intrusion:
465 optimising ACUAINTRUSION and selecting cation exchange coefficients with
466 PHREEQC." *J. Hydrol*. 510: 59-69.

467 Broholm, K., Hansen, A.B., Jorgensen, P.R., Arvin, E., Hansen, M. 1999. "Transport
468 and biodegradation of creosote compounds in a large, intact, fractured clayey till
469 column." *J. Contam. Hydrol.* 39 (3-4): 331-348.
470 Caporaso, J.G., Lauber, C.L., Walters, W.A., Berg-Lyons, D., Huntley, J., Fierer, N.,
471 Owens, S.M., Betley, J., Fraser, L., Bauer, M., Gormley, N., Gilbert, J.A., Smith, G.,
472 Knight, R. 2012. "Ultra-high-throughput microbial community analysis on the
473 Illumina HiSeq and MiSeq platforms." *Isme J.* 6 (8): 1621-1624.
474 Caporaso, J.G., Lauber, C.L., Walters, W.A., Berg-Lyons, D., Lozupone, C.A.,
475 Turnbaugh, P.J., Fierer, N., Knight, R. 2011. "Global patterns of 16S rRNA diversity
476 at a depth of millions of sequences per sample." *P. Natl. Acad. Sci. USA* 108:
477 4516-4522.
478 Carboneras, B., Villaseñor, J., Fernandez-Morales, F.J. 2017. "Modelling aerobic
479 biodegradation of atrazine and 2, 4-dichlorophenoxy acetic acid by mixed-cultures."
480 *Bioresour. Technol.* 243: 1044-1050.
481 Carvajal, A., Akmirza, I., Navia, D., Pérez, R., Muñoz, R., Lebrero, R. 2018. "Anoxic
482 denitrification of BTEX: biodegradation kinetics and pollutant interactions." *J.*
483 *Environ. Manage.* 214: 125-136.
484 Chen, T.Y., Kao, C.M., Chiou, H.Y., Yu, Y.T., Sung, W.P. 2012. "Application of
485 oxygen-releasing material to enhance in situ aerobic bioremediation." *Adv. Mater.*
486 *Res.*
487 Chen, Z.Q., McTernan, W.F. 1992. "Multi-substrate, multi-option groundwater

488 transport model." *J. Contam. Hydrol.* 11 (3-4): 215-244.

489 Cobas, M., Ferreira, L., Sanromán, M.A., Pazos, M. 2014. "Assessment of sepiolite as
490 a low-cost adsorbent for phenanthrene and pyrene removal: kinetic and equilibrium
491 studies." *Ecol. Eng.* 70: 287-294.

492 Cogle, A.L., Saffigna, P.G., Strong, W.M. 1989. "Carbon transformations during
493 wheat straw decomposition." *Soil Biol. Biochem.* 21 (3): 367-372.

494 Ebihara, T., Bishop, P.L. 2002. "Influence of supplemental acetate on bioremediation
495 for dissolved polycyclic aromatic hydrocarbons." *J. Environ. Eng. (New York)* 128 (6):
496 505-513.

497 Ferreira, L., Cobas, M., Tavares, T., Sanromán, M.A., Pazos, M. 2013. "Assessment
498 of Arthrobacter viscosus as reactive medium for forming permeable reactive
499 biobarrier applied to PAHs remediation." *Environ. Sci. Pollut. Res.* 20 (10):
500 7348-7354.

501 Folch, A., Vilaplana, M., Amado, L., Vicent, T., Caminal, G. 2013. "Fungal permeable
502 reactive barrier to remediate groundwater in an artificial aquifer." *J. Hazard. Mater.*
503 262: 554-560.

504 Gandhi, S., Oh, B.T., Schnoor, J.L., Alvarez, P.J.J. 2002. "Degradation of TCE, Cr(VI),
505 sulfate, and nitrate mixtures by granular iron in flow-through columns under different
506 microbial conditions." *Water Res.* 36 (8): 1973-1982.

507 Geng, X.L., Boufadel, M.C., Wrenn, B. 2013. "Mathematical modeling of the
508 biodegradation of residual hydrocarbon in a variably-saturated sand column."

509 *Biodegradation* 24 (2): 153-163.

510 Hannam, M.L., Bamber, S.D., Galloway, T.S., Moody, A.J., Jones, M.B. 2010.
511 "Effects of the model PAH phenanthrene on immune function and oxidative stress in
512 the haemolymph of the temperate scallop Pecten maximus." *Chemosphere* 78 (7):
513 779-784.

514 Haritash, A.K., Kaushik, C.P. 2009. "Biodegradation aspects of Polycyclic Aromatic
515 Hydrocarbons (PAHs): A review." *J. Hazard. Mater.* 169 (1-3): 1-15.

516 Kohfahl, C., Pekdeger, A. 2006. "Rising groundwater tables in partly oxidized pyrite
517 bearing dump-sediments: Column study and modelling approach." *J. Hydrol.* 331
518 (3-4): 703-718.

519 Krishnan, J., Kishore, A.A., Suresh, A., Madhumeetha, B., Prakash, D.G. 2017.
520 "Effect of pH, inoculum dose and initial dye concentration on the removal of azo dye
521 mixture under aerobic conditions." *Int. Biodeterior. Biodegradation* 119: 16-27.

522 Lee, Y.-Y., Fan, C. 2020. "Mechanistic exploration of the catalytic modification by
523 co-dissolved organic molecules for micropollutant degradation during fenton
524 process." *Chemosphere* 258: 127338.

525 Lin, C.W., Wu, C.H., Guo, P.Y., Chang, S.H. 2017. "Innovative encapsulated
526 oxygen-releasing beads for bioremediation of BTEX at high concentration in
527 groundwater." *J. Environ. Manage.* 204: 12-16.

528 Liu, C.C., Chen, X.H., Mack, E.E., Wang, S., Du, W.C., Yin, Y., Banwart, S.A., Guo,
529 H.Y. 2019. "Evaluating a novel permeable reactive bio-barrier to remediate

530 PAH-contaminated groundwater." *J. Hazard. Mater.* 368: 444-451.

531 Lokshina, L.Y., Vavilin, V.A., Kettunen, R.H., Rintala, J.A., Holliger, C.,
532 Nozhevnikova, A.N. 2001. "Evaluation of kinetic coefficients using integrated Monod
533 and Haldane models for low-temperature acetoclastic methanogenesis." *Water Res.* 35
534 (12): 2913-2922.

535 McClure, P.D., Sleep, B.E. 1996. "Simulation of bioventing for soil and ground-water
536 remediation." *J. Environ. Eng.* 122 (11): 1003-1012.

537 Mohanty, S.K., Valenca, R., Berger, A.W., Yu, I.K.M., Xiong, X.N., Saunders, T.M.,
538 Tsang, D.C.W. 2018. "Plenty of room for carbon on the ground: Potential applications
539 of biochar for stormwater treatment." *Sci. Total Environ.* 625: 1644-1658.

540 Moscoso, F., Deive, F.J., Longo, M.A., Sanroman, M.A. 2012. "Technoeconomic
541 assessment of phenanthrene degradation by Pseudomonas stutzeri CECT 930 in a
542 batch bioreactor." *Bioresour. Technol.* 104: 81-89.

543 Obiri-Nyarko, F., Kwiatkowska-Malina, J., Malina, G., Kasela, T. 2015.
544 "Geochemical modelling for predicting the long-term performance of zeolite-PRB to
545 treat lead contaminated groundwater." *J. Contam. Hydrol.* 177: 76-84.

546 Pantić, K., Bajić, Z.J., Veličković, Z.S., Nešić, J.Z., Đolić, M.B., Tomić, N.Z.,
547 Marinković, A.D. 2019. "Arsenic removal by copper-impregnated natural mineral tufa
548 part II: a kinetics and column adsorption study." *Environ. Sci. Pollut. Res.*: 1-19.

549 Safdari, M.S., Kariminia, H.R., Rahmati, M., Fazlollahi, F., Polasko, A., Mahendra, S.,
550 Wilding, W.V., Fletcher, T.H. 2018. "Development of bioreactors for comparative

551 study of natural attenuation, biostimulation, and bioaugmentation of
552 petroleum-hydrocarbon contaminated soil." *J. Hazard. Mater.* 342: 270-278.
553 Sponza, D.T., Gok, O. 2011. "Effects of sludge retention time and biosurfactant on the
554 treatment of polyaromatic hydrocarbon (PAH) in a petrochemical industry
555 wastewater." *Water Sci. Technol.* 64 (11): 2282-2292.
556 Tebes-Stevens, C., Valocchi, A.J., VanBriesen, J.M., Rittmann, B.E. 1998.
557 "Multicomponent transport with coupled geochemical and microbiological reactions:
558 model description and example simulations." *J. Hydrol.* 209 (1-4): 8-26.
559 Verce, M.F., Ulrich, R.L., Freedman, D.L. 2000. "Characterization of an isolate that
560 uses vinyl chloride as a growth substrate under aerobic conditions." *Appl. Environ.*
561 *Microbiol.* 66 (8): 3535-3542.
562 Waigi, M.G., Kang, F.X., Goikavi, C., Ling, W.T., Gao, Y.Z. 2015. "Phenanthrene
563 biodegradation by sphingomonads and its application in the contaminated soils and
564 sediments: A review." *Int. Biodeterior. Biodegradation* 104: 333-349.
565 Wang, P., Zhang, Y.M., Jin, J., Wang, T.H., Wang, J., Jiang, B.Y. 2020. "A
566 high-efficiency phenanthrene-degrading Diaphorobacter sp. isolated from
567 PAH-contaminated river sediment." *Sci. Total Environ.*: 140455.
568 Wu, C.F., Shimaoka, T., Nakayama, H., Komiya, T. 2015. "Kinetics of nitrous oxide
569 production by denitrification in municipal solid waste." *Chemosphere* 125: 64-69.
570 Yeh, C.H., Lin, C.W., Wu, C.H. 2010. "A permeable reactive barrier for the
571 bioremediation of BTEX-contaminated groundwater: Microbial community

572 distribution and removal efficiencies." *J. Hazard. Mater.* 178 (1-3): 74-80.

573 Zhang, J.M., Jiang, X.C., Feng, C.P., Hao, H.L. 2017. "Wheat straw, sawdust, and
574 biodegradable plastics as potential carbon sources for synthetic nitrate-polluted
575 groundwater column denitrification." *Desalination Water Treat.* 77: 321-330.

576 Zhang, M., Feng, Y.D., Zhang, D.Y., Dong, L.F., Pan, X.L. 2019.
577 "Ozone-encapsulated colloidal gas aphrons for in situ and targeting remediation of
578 phenanthrene-contaminated sediment-aquifer." *Water Res.* 160: 29-38.

579 Zhang, W.C., Zhu, J.Q., Zhou, X.G., Li, F.H. 2018. "Effects of shallow groundwater
580 table and fertilization level on soil physico-chemical properties, enzyme activities,
581 and winter wheat yield." *Agr. Water Manage.* 208: 307-317.

582

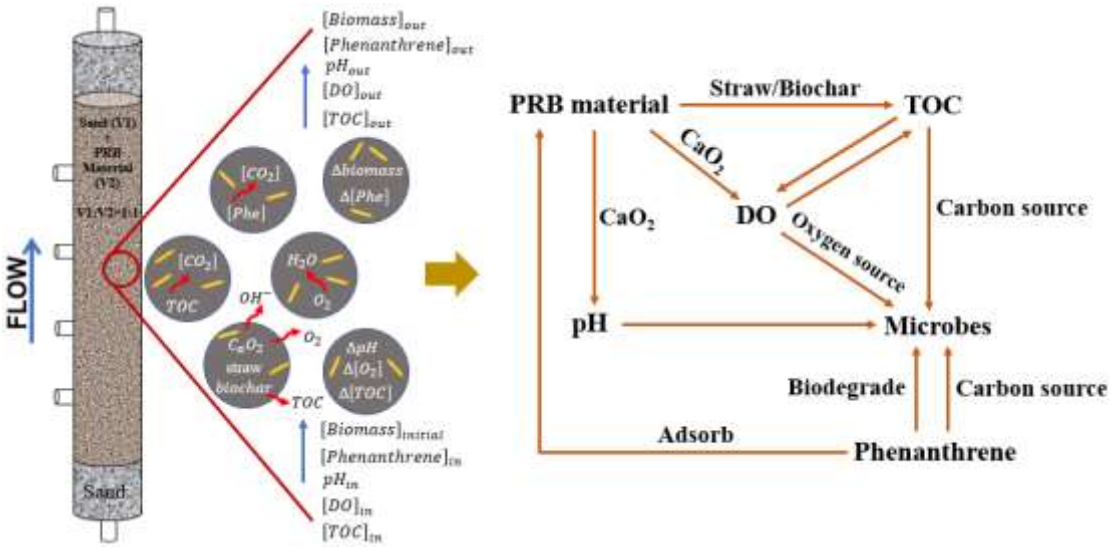

Fig. 1. A conceptual model for modelling the process of the column experiment.

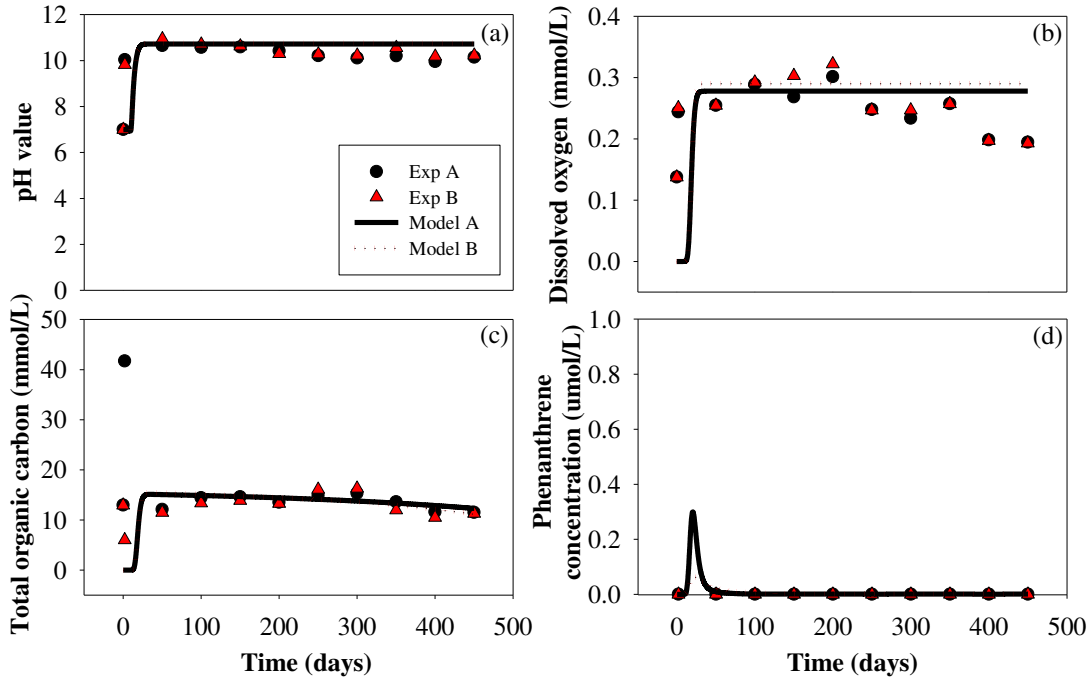

Fig. 2. Simulated (lines) and experimental (symbols) results for variations in (a) pH value, (b) dissolved oxygen, (c) total organic carbon, and (d) phenanthrene concentration in the effluents of the columns A and B.

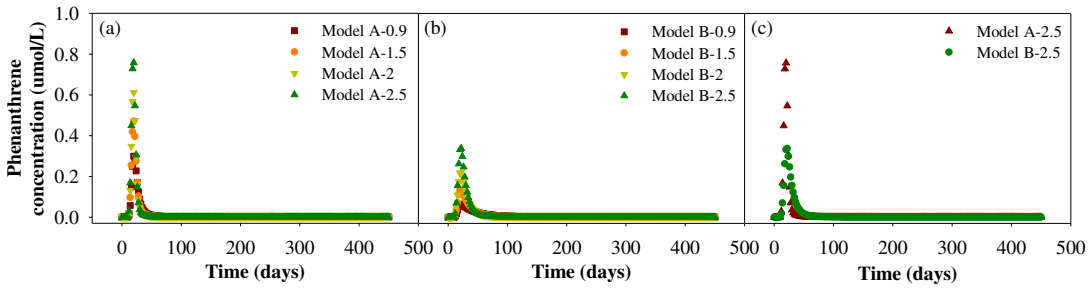

Fig. 3. Modelling results for the change of phenanthrene concentration in the effluents of (a) column A and (b) column B when the initial concentration of phenanthrene was 0.9, 1.5, 2, and 2.5 mg/L, respectively. (c) The comparison of modelling results for phenanthrene concentration in the effluents of columns A and B (with an initial phenanthrene concentration of 2.5 mg/L).

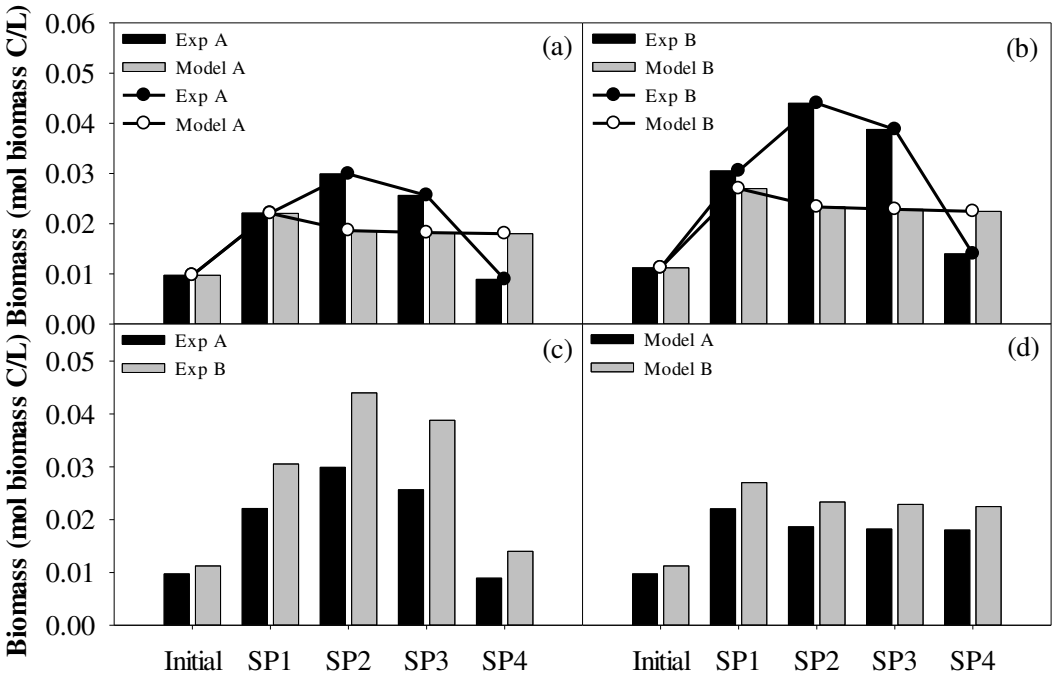

Fig. 4. The comparison of simulated and experimental results of the biomass from the initial materials and samples collected from ports SP1-4 of columns (a) A and (b) B. The (c) experimental and (d) simulated results for the biomass in columns A and B.

Table 1. General characteristics of raw materials used in the PRB material

Raw material	Fractionation	Particle size range
Wood brick	granule	2-4 mm
Wheat straw	powder	550-700 μm
Coconut shell biochar	powder	150-180 μm
Calcium peroxide (70%)	powder	150-180 μm
Attapulgite	powder	150-180 μm
Diatomite	powder	180-270 μm
Cement	powder	150-180 μm
Sodium alginate	powder	150-180 μm

Table 2. Characteristics of columns A and B used in the simulations

Parameter	Column A	Column B
Column volume (mL)	628	628
PRB material (g)	250.5	238.5
Quartz sand (g)	663.5	677
Pore volume (mL)	148.2	151.3
Porosity (%)	23.6	24.1
Hydraulic conductivity (m d^{-1})	0.48	0.48
Residence time (h)	24.93	24.93

Table 3. The ADR equations for the local change of species concentrations in porewater or solids

Species	Phase	ADR equation
Phenanthrene	porewater	$\frac{\partial C_{phen,pw}}{\partial t} = -v\frac{\partial C_{phen,pw}}{\partial x} + D_L\frac{\partial^2 C_{phen,pw}}{\partial x^2} + R_{phen,sorp} + R_{phen,bio}$ $R_{phen,sorp} = -k_m\left(C_{phen,pw} - \frac{C_{phen,s}}{K_d}\right)$ $R_{phen,bio} = -\frac{\mu_{max,phen}X_{phen}}{14Y_{X_{phen}}}\frac{C_{phen,pw}}{K_{phen}+C_{phen,pw}}\frac{C_{ox,pw}}{K_{ox}+C_{ox,pw}}$
	solid	$\frac{\partial C_{phen,s}}{\partial t} = -R_{phen,sorp}K_d$ $R_{phen,sorp} = -k_m\left(C_{phen,pw} - \frac{C_{phen,s}}{K_d}\right)$
TOC	porewater	$\frac{\partial C_{TOC,pw}}{\partial t} = -v\frac{\partial C_{TOC,pw}}{\partial x} + D_L\frac{\partial^2 C_{TOC,pw}}{\partial x^2} + R_{TOC,bio}$ $R_{TOC,bio} = -\frac{\mu_{max,TOC}X_{TOC}}{Y_{X_{TOC}}}\frac{C_{TOC,pw}}{K_{TOC}+C_{TOC,pw}}\frac{C_{ox,pw}}{K_{ox}+C_{ox,pw}}$
Oxygen	porewater	$\frac{\partial C_{ox,pw}}{\partial t} = -v\frac{\partial C_{ox,pw}}{\partial x} + D_L\frac{\partial^2 C_{ox,pw}}{\partial x^2} + R_{ox} + 16.5R_{phen,bio} + R_{TOC,bio}$ $R_{ox} = \lambda$ $R_{phen,bio} = -\frac{\mu_{max,phen}X_{phen}}{14Y_{X_{phen}}}\frac{C_{phen,pw}}{K_{phen}+C_{phen,pw}}\frac{C_{ox,pw}}{K_{ox}+C_{ox,pw}}$ $R_{TOC,bio} = -\frac{\mu_{max,TOC}X_{TOC}}{Y_{X_{TOC}}}\frac{C_{TOC,pw}}{K_{TOC}+C_{TOC,pw}}\frac{C_{ox,pw}}{K_{ox}+C_{ox,pw}}$
Biomass	solid	$\frac{\partial C_{bm,s}}{\partial t} = \frac{\partial X_{phen}}{\partial t} + \frac{\partial X_{TOC}}{\partial t} = R_{bm,phen} + R_{bm,TOC}$ $R_{bm,phen} = -14Y_{X_{phen}}R_{phen,bio} - bX_{phen}$ $R_{bm,TOC} = -Y_{X_{TOC}}R_{TOC,bio} - bX_{TOC}$

Note: (mol L^{-1}) → $C_{phen,pw}$; K_{phen}; $C_{ox,pw}$; K_{ox}; $C_{TOC,pw}$; K_{TOC}; $C_{bm,s}$
(mol biomass C L^{-1}) → X_{phen}; X_{TOC} (mol biomass C L^{-1} s^{-1}) → $R_{bm,phen}$; $R_{bm,TOC}$
(mol L^{-1} s^{-1}) → $R_{phen,sorp}$; $R_{phen,bio}$; $R_{TOC,bio}$; R_{ox}; λ
(mol biomass C/mol phenanthrene C) → $Y_{X_{phen}}$ (mol biomass C/mol TOC C) → $Y_{X_{TOC}}$
(s^{-1}) → k_m; $\mu_{max,phen}$; $\mu_{max,TOC}$; b (m^2 s^{-1}) → D_L (s) → t
(m s^{-1}) → v (m) → x (mol g^{-1}) → $C_{phen,s}$ (L g^{-1}) → K_d

Table 4. Model transport parameters

Parameter	Value	Unit
Cells	10	-
Lengths	10×0.04	m
Shifts	225	-
Time_step	172800	s
Flow_direction	Forward	-
Boundary_conditions	Flux-flux	-
Diffusion_coefficient	0.03×10^{-9}	$m^2\ s^{-1}$
Dispersivities	0.005	m
Correct_disp	True	-

Table 5. Modelling parameters for the column experiment

Parameter	Column A	Column B
Phenanthrene adsorption	k_m = 2.63×10^{-4} (Pantić et al. 2019); K_d = 5.33×10^{-4} (Tebes-Stevens et al. 1998)	k_m = 4.5×10^{-4} (Pantić et al. 2019); K_d = 4.27×10^{-4} (Tebes-Stevens et al. 1998)
Phenanthrene biodegradation	$\mu_{max,phen}$ = 3.33×10^{-6} (Krishnan et al. 2017); K_{phen} = 7.1×10^{-6} (McClure and Sleep 1996); $Y_{X_{phen}}$ = 0.44 (This value fit well with the experimental data); K_{ox} = 6.25×10^{-6} (Tebes-Stevens et al. 1998)	$\mu_{max,phen}$ = 8.22×10^{-7} (Carboneras et al. 2017); K_{phen} = 7.1×10^{-6} (McClure and Sleep 1996); $Y_{X_{phen}}$ = 0.53 (This value fit well with the experimental data); K_{ox} = 6.25×10^{-6} (Tebes-Stevens et al. 1998)
TOC consumption	$\mu_{max,TOC}$ = 5.1×10^{-8} (Lokshina et al. 2001); K_{TOC} = 7.1×10^{-6} (McClure and Sleep 1996); $Y_{X_{TOC}}$ = 0.932 (This value fit well with the experimental data); K_{ox} = 6.25×10^{-6} (Tebes-Stevens et al. 1998)	$\mu_{max,TOC}$ = 5.56×10^{-8} (Verce et al. 2000); K_{TOC} = 7.1×10^{-6} (McClure and Sleep 1996); $Y_{X_{TOC}}$ = 0.954 (This value fit well with the experimental data); K_{ox} = 6.25×10^{-6} (Tebes-Stevens et al. 1998)
Biomass	b = 1.16×10^{-8} (Chen and McTernan 1992)	b = 1.16×10^{-8} (Chen and McTernan 1992)